Acta Crystallographica Section D
Biological Crystallography
ISSN 0907-4449

Structure of the histone-core octamer in KCl/phosphate crystals at 2.15 Å resolution

L. Chantalat,[a] J. M. Nicholson,[b] S. J. Lambert,[c] A. J. Reid,[c] M. J. Donovan,[c] C. D. Reynolds,[c] C. M. Wood[c] and J. P. Baldwin[b,c]*

[a]Structural Biology, Galderma RandD, 635 Route des Lucioles, BP 87F-06902 Sophia Antipolis CEDEX, France, [b]Synchrotron Radiation Department, Daresbury Laboratory, Warrington, Cheshire WA4 4AD, England, and [c]School of Biomolecular Scienecs, John Moores University, Byrom Street, Liverpool L3 3AF, England

Correspondence e-mail: j.p.baldwin@dl.ac.uk

Received 1 July 2002
Accepted 29 May 2003

PDB Reference: histone-core octamer, 1hq3, r1hq3sf.

The structure of the native chicken histone octamer, crystallized in 2 *M* KCl, 1.35 *M* potassium phosphate pH 6.9, has been refined at 2.15 Å resolution to a final *R* factor of 21.4% and an $R_{\rm free}$ of 25.2%. Unique crystal-packing interactions between histone-core octamers are strong and one of them (area 4000 Å^2) involves two chloride ions and direct interactions between six acidic amino-acid residues on one octamer and the equivalent number of basic residues on the next. These interactions are on the structured part of the octamer (not involving tails). Five phosphate ions, 23 chloride ions and 437 water molecules have been identified in the structure. The phosphate and some chloride ions bind to basic amino-acid residues that interact with DNA in the nucleosome. The binding of most of the anions and the packing interactions are unique to these crystals. In other respects, and including the positions of four chloride ions, the octamer structure is very close to that of octamers in nucleosome-core particle crystals, particularly with respect to 'docking' sequences of the histone H2As and H4s. These sequences together with the H2B–H4 four-helix bundles stabilize the histone structure in the nucleosome and prevent the dissociation of the (H2A–H2B) dimers from the $(H3–H4)_2$ tetramer. Possible reasons why this happens at high salt in the absence of DNA are given.

1. Introduction

The present understanding of the functions of histone proteins and nucleosomes and the implications of histone post-translational modifications and nucleosome remodelling in the control of transcription and other cellular processes has been reviewed recently (Wolffe, 1999; Wu & Grunstein, 2000; Rice & Allis, 2001; Akey & Luger, 2003). The structures of the nucleosome-core particle and its associated histone octamer (Richmond *et al.*, 1984; Arents *et al.*, 1991; Wang *et al.*, 1994; Luger *et al.*, 1997; Luger & Richmond, 1998; Harp *et al.*, 2000; Suto *et al.*, 2000; White *et al.*, 2001; Davey *et al.*, 2002) have been extensively studied and this has provided information essential for trying to understand their functions in relation to structure at the atomic level.

Even though the two copies of the histone hetero-typic dimers in the histone octamer have the same sequence (Fig. 1), the nature of DNA binding in the nucleosome (Luger & Richmond, 1998; Davey *et al.*, 2002) and asymmetries in octamer structure necessitate labelling each of the two copies differently. Unprimed and primed labels are used, as in Luger *et al.* (1997).

Each histone-core octamer is composed of two histone dimers, (H2A–H2B) plus (H2A′–H2B′), and one tetramer, (H4–H3).(H3′–H4′), each being formed by histone-fold pairing (Arents *et al.*, 1991). The four histone-fold pairs of the

octamer are connected together by three four-helix bundles in the order (H2A–H2B)–(H4–H3)–(H3′–H4′)–(H2B′–H2A′), so that the symmetry of the octamer is approximately twofold. Combined, these elements form a left-hand helical track (Fig. 2*a*) on the outside of which ∼121 base pairs of DNA coil with a super-helical pitch of 24 Å (Fig. 1*a* of Luger *et al.*, 1997). The conserved histone-fold structural motif contains α-helices: α1, α2 and α3 with three, eight and three turns, respectively. Loops L1 and L2 separate α-helices to form an α1–L1–α2–L2–α3 domain (Fig. 1, Arents *et al.*, 1991).

α-Helices other than those in the histone-fold pairing are as follows.

(i) The N-terminus, or αN helix (Figs. 1 and 2*a*), on histone H3 (also for H3′), is stabilized by a 'molecular cluster' and by bound water molecules to the other parts of the histone octamer (Figs. 2*b* and 2*c*). The αN helix of histone H3 extends from the α1 helix by a long loop LH3, allowing it to cross over into the H2A′ domain, as shown in Fig. 2(*a*). In this way, an extra section of DNA (∼13 base pairs) is allowed to enter the nucleosome core particle over the αN helix of histone H3 to continue winding over the histone-fold pair (H2A′–H2B′) (Fig. 2*a* and Fig. 1*a* of Luger *et al.*, 1997). Equivalently, a section of DNA exits over the αN helix of histone H3′ to make the 146 total base pairs of the nucleosome core particle.

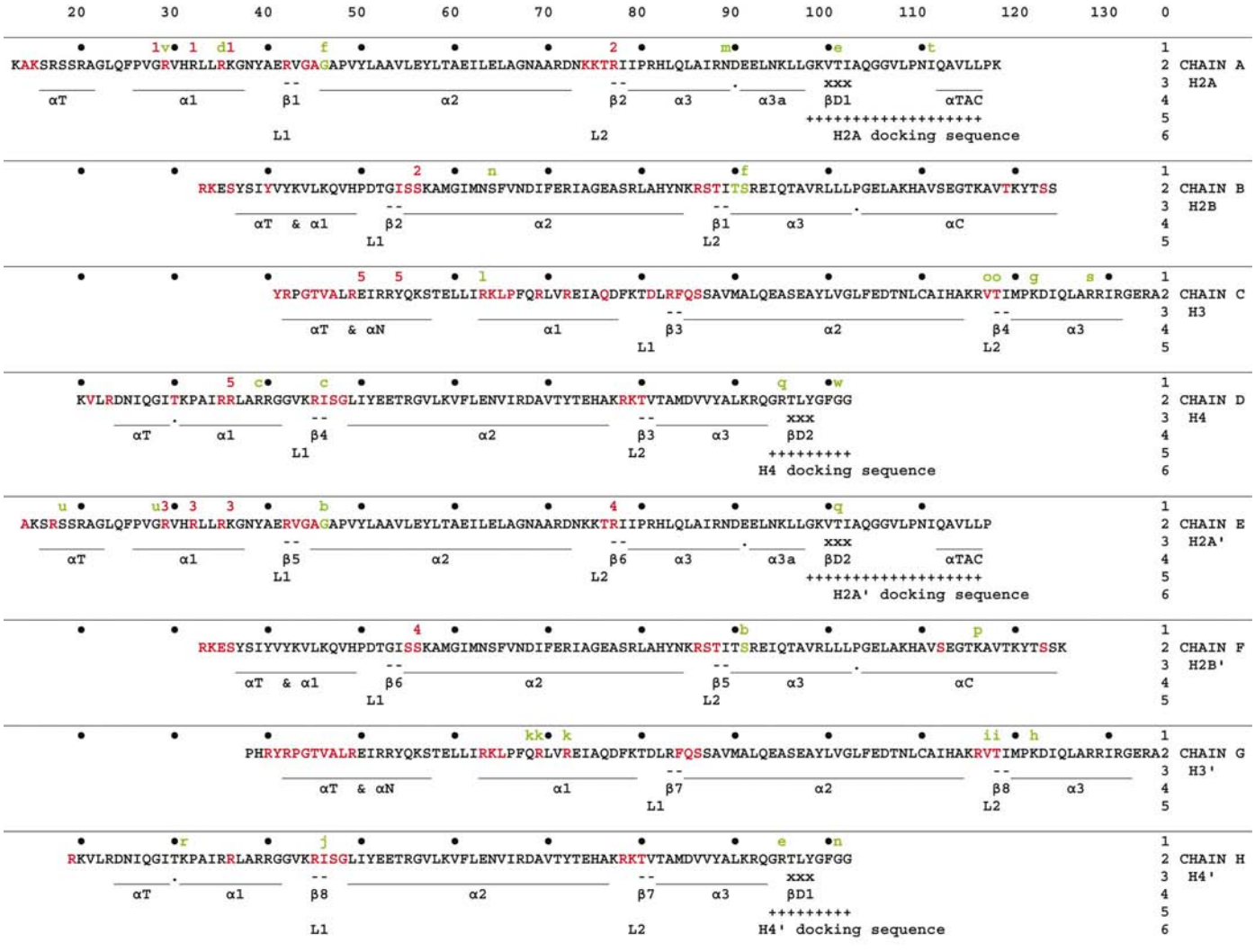

Figure 1
The sequence of amino-acid residues for the proteins of the histone octamer and related structural details for the KCl/phosphate crystal structure. Histone N-terminal tail regions extend to Lys15 on the H2As, Ser36 on the H2Bs, Tyr41 on the H3s and Arg23 on the H4s. The C-terminal tails of the H2As extend from Pro117. Most of the amino-acid residues in the tails in our structure are disordered. There are lines of information, labelled 0 to 6, for each of the eight histone proteins in the figure, identifying details of structure correlated with the amino-acid sequence. Line 0: the sequence number of the amino-acid residue. Line 1: black spheres indicate ten amino-acid residue intervals. Green lower-case letters, a–w, indicate the positions of 23 chloride ions. Red numbers, 1–5, indicate the positions of the phosphate ions. Line 2: the capital letters are the single-letter code for the amino-acid sequence. The letters are black, but are coloured red where there are DNA-binding sites in the nucleosome-core particle structure of Harp *et al.* (2000) and green for where the chloride ions bind in that structure. Line 3: the dashes show the positions of short β-sheet regions between the histone-fold pair loop regions. The xxx indicate β-sheet regions between the H2A′ and H4, and the H2A and H4′ docking sequences. The continuous underlines indicate the positions of α-helices. Line 4: symbols for the elements of structure: 'α' for α-helices, 'β' for short parallel β-sheet regions and 'βD' for the two docking β-sheets. Line 5, +++ indicates the docking sequences of H2A, H4, H2A′ and H4′. Lines 6: labels for the docking sequences and loop regions are given.

(ii) The C-terminal, or αC helices, one for each histone H2B (Fig. 1 and shown magenta in Fig. 2*a*), are prominent features when viewed along the axes of the DNA supercoiling. The αC helix of histone H2B has a clearly defined hydrophobic surface, allowing it to bind back into the (H2A–H2B) dimer.

(iii) The histone N-termini have lysine- and arginine-rich DNA-binding regions that comprise about 28% of the

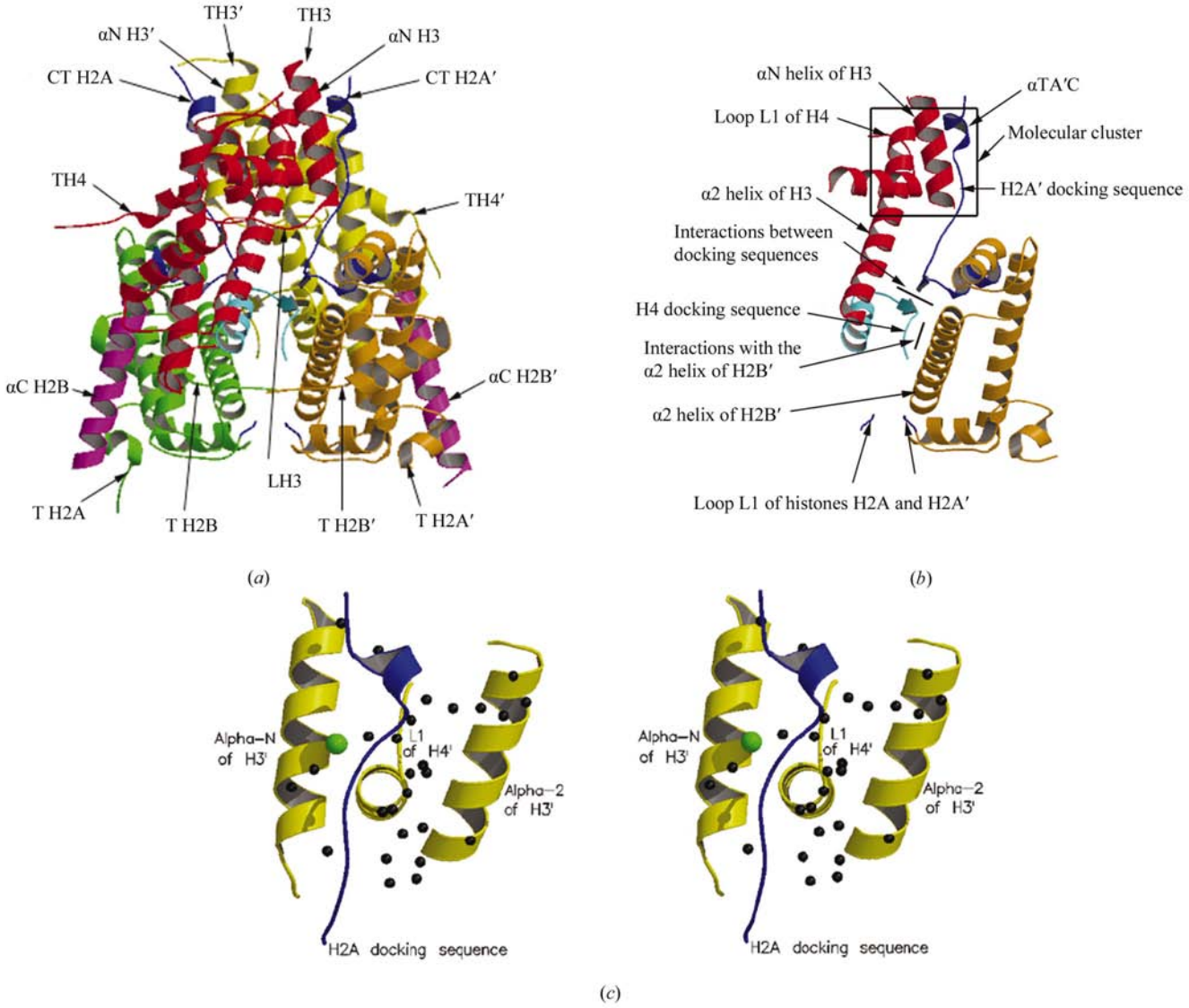

Figure 2
Colour code: red helix, αN of histone H3; orange histone-fold pair, H2A′–H2B′; Yellow histone-fold pair, H3′–H4′; red histone-fold pair, H3–H4; green histone-fold pair, H2A–H2B; long (red) loop, LH3; magenta, αC helix of histones H2B; black spheres. water molecules; green spheres, chloride ions. (*a*) The histone octamer in KCl/phosphate viewed with the pseudo-twofold axis vertical and the axis of would-be DNA coiling horizontally. The labels starting with a 'T' correspond to the last amino-acid residue in the N-terminal tail of the appropriate histones. The label CT H2A indicates the first residue in the C-terminal tails of histones H2A. These residues are next in sequence to α helices in the 'structured' part of the octamer, which lock them in position. LH3 is the loop which allows the αN helix of histone H3 to be 'switched' to the right of the figure. (*b*) An enlarged section of Fig. 2(*a*), showing the three ways that the histone-pair (H2A′–H2B′) docks against the (H3–H4) histones in forming the helical histone track. The square box shows the so-called molecular cluster formed by hydrogen bonding between the H2A′ docking sequence (residues Ala103–Leu115), the αN helix of H3 (residues Gly55 and Thr58), the α2 helix of H3 (residue Glu94) and part of the L1 loop of histone H4 (residue Lys44). See also Fig. 2(*c*). This molecular cluster stabilizes the αN helix of H3, to control DNA-entry and DNA-exit binding, and locates the starting points of the N-terminal tail of H3 and the C-terminal tail of H2A′. Interactions between regions called docking sequences (see also Figs. 1 and 5*c*) occur as a result of hydrogen bonds between residues Arg95–Tyr98 of H4 and residues Lys99–Thr103 of H2A′. These interactions form a three amino-acid parallel β-sheet (Fig. 1). Residues Tyr98–Gly102 of the H4 docking sequence form hydrogen bonds with the α2 histone-fold helix of histone H2B′ (residues Ser64 and Asp68). There are numerous non-covalent interactions which link the H2A′ docking sequence and the H4 docking sequence to their own side of the helical track (see §1). Similar cross-ties also occur for the H2A and H4′ docking sequences. (*c*) A stereo figure showing how the position of the αN helix of histone H3′, relative to the (H2A. H2B) histone pair, is determined by the H2A docking sequence (residues Ala103–Leu115 of H2A), which forms a molecular cluster with this αN helix (residues Gly55 and Thr58 of H3′), the α2 helix of H3′ (residue Glu94) and part of the L1 loop of histone H4′ (residue Lys44). The clustering is *via* many hydrogen bonds, both direct and *via* waters. Chloride ion t is also shown.

histone amino-acid residues (Fig. 1). These tails are largely disordered in histone-octamer crystals and partially ordered in nucleosome-core particle crystals (Luger *et al.*, 1997). They end abruptly at the start of α-helices (Figs. 1 and 2*a*): helix α1 for each H2B, αN for each H3, αT for each H2A and αT for each H4. The αT helices of H2A and H4 in Fig. 2(*a*) are short 'tail-positioning' helices connected by loops from the α1 helices of histones H2A and H4, respectively.

The C-terminal regions of histones H2B and H3 end in α-helices (apart from the last one or two residues), while the α-helices αTAC, shown in Fig. 2(*b*) and in Fig. 1, position the start of each H2A C-terminal tail. Although the histone pair (H2A–H2B) is coupled to the (H3–H4) pair by a four-helix bundle between the H4 and H2B molecules, it is held in position and stabilized by interactions with the (H3′–H4′) histone pair. The docking, as shown in Fig. 2(*b*), is *via* interactions involving two specific sequences of amino-acid residues that are referred to as 'docking sequences': Gln93 to the terminus (Gly102) of histone H4 (H4 docking sequence) and Leu97 to the end of the C-tail-positioning helix (Leu115) of histone H2A′ (H2A′ docking sequence). Part of the H2A′ docking sequence stabilizes the αN helix of H3 in the molecular cluster shown in Figs. 2(*b*) and 2(*c*), whereas another part, Lys99–Thr101, forms a three amino-acid residue parallel β-sheet with residues Thr96–Tyr98 of the H4 docking sequence (Figs. 1 and 2*b*). The residues Gly97 to Gly102 of the H4 docking sequence interact with the α2 helix of histone H2B (Fig. 1) to complete the three types of interaction shown in Fig. 2(*b*). The (H2A–H2B) and (H3′–H4′) histone dimers interact in a similar way.

22 base pairs of additional DNA, complexed with linker histone H1 (also H5 in avian erythrocytes) and 0 to ∼70 base pairs (species-dependent) of linker DNA complete the nucleosome. Chains of nucleosomes zigzag from one nucleosome to the next and fold into higher order structures (Finch & Klug, 1976; Thoma *et al.*, 1979; Woodcock & Dimitrov, 2001). These are thought to undergo further ordering into looped domains that are associated with the genes of eukaryotic chromosomes.

The DNA/histone-octamer complex is stable in inactive regions of chromatin in cell nuclei and in low ionic strength buffers *in vitro*. However, when DNA is removed at low ionic strength, each octamer dissociates into one $(H3–H4)_2$ tetramer and two (H2A–H2B) dimers (Eickbush & Moudrianakis, 1978). Nevertheless, the octamer remains ntact in high salt; for example, in ammonium sulfate (Arents *et al.*, 1991). The histone octamer is generally fairly stable in 2 *M* KCl, with some dissociation, and can be stable in some species (Moehs *et al.*, 1992). In the present study the octamer is stable when extracted in 2 *M* KCl, 0.2 *M* K_2HPO_4, 0.2 *M* KH_2PO_4. Crystals diffracting to high resolution have been produced in KCl/phosphate (Carter *et al.*, 1996; Lambert *et al.*, 1999). The present paper reports the refined crystal structure of the histone octamer at 2.15 Å resolution, describes the detailed structure of the protein complex, its crystal packing, anion interactions and gives a comparison with previously published structures of both the histone octamer and the nucleosome-core particle.

2. Experimental

2.1. Crystallization and sample handling

Histone octamers were prepared in 2 *M* KCl, 0.2 *M* K_2HPO_4, 0.2 *M* KH_2PO_4, dialysed against 0.475 *M* K_2HPO_4, 0.475 *M* KH_2PO_4 at 277 K overnight and centrifuged at 13 000*g* for 1 h. The supernatant (adjusted to contain histone octamers at 20 mg ml^{-1}, OD_{278} = 9) was partitioned into 50 µl crystallization cells and dialysed into the 2 *M* KCl, 0.675 *M* K_2HPO_4, 0.675 *M* KH_2PO_4. The crystal quality was very sensitive to pH, which in turn was dependent on a given solvent batch. The optimum pH, close to 6.9, was achieved by small variations of the monobasic and dibasic phosphate ions, while keeping the total phosphate concentration at 1.35 *M*. The chick-erythrocyte histone octamers described herein: $(H3–H4)_2$. 2(H2A–H2B) in 2 *M* KCl, 0.675 *M* K_2HPO_4, 0.675 *M* KH_2PO_4 without reducing agents or oxidizing agents, formed hexagonal crystals, space group $P6_5$, with unit-cell parameters $a = b = 158.6$, $c = 102.5$ Å and have one octamer in the asymmetric unit (Lambert *et al.*, 1999).

Large 2–3 mm long crystal needles grew within a few months. These were removed from the dialysis cells on loops made from the very finest strands of unwaxed dental floss. They were briefly soaked progressively in crystallization buffers containing up to 20% glycerol and dropped into vials containing liquid nitrogen. The crystals were transferred, for data acquisition, from vials placed directly in the cryostream of the X-ray apparatus at 100 K.

2.2. Data collection, structure determination and refinement

Data were collected on beamline 7.2 of the Daresbury Laboratory Synchrotron Radiation Source as previously reported (Carter *et al.*, 1996; Lambert *et al.*, 1999). Three data sets were processed using the *HKL* program suite (Otwinowski & Minor, 1997), yielding merging R values between 5 and 7% overall and approximately 30% in the 2.25–2.15 Å highest resolution shell. The three data sets were combined, giving a merging R of 7.1% (33% in the highest resolution shell), 74 806 reflections (corresponding to a completeness of 97.4% with 97.1% in the highest resolution shell), a multiplicity of 2.26 (2.16 in the highest resolution shell) and a mosaicity in the range 0.25–0.45°. The percentage of reflections with $I > 3\sigma(I)$ was 75.8% (56.6% in the highest resolution shell).

The structure was determined by the molecular-replacement method using the program *AMoRe* (Navaza, 1994) and the 3.1 Å resolution structure of the histone octamer (Arents *et al.*, 1991; PDB code 1hio) as a search model. After rigid-body refinement with *CNS* (Brünger *et al.*, 1998), the R_{work} and the R_{free} (6% of the data) had both decreased by 2% to 36.4 and 38.7%, respectively, at 2.8 Å. Refinement of coordinates and thermal parameters was performed using all data to 2.15 Å, with the maximum-likelihood target function (Pannu

Table 1
Data-collection and refinement statistics.

Values in parentheses refer to the highest resolution shell: 2.25–2.15 Å.

(*a*) Histone-core octamer (KCl)

Crystal dimensions (mm)	2.0 × 0.2× 0.2
X-ray source	Station 7.2, SRS Daresbury, UK
Detector	MAR image plate (300 mm)
Wavelength (Å)	1.488
Temperature (K)	100
Rotation range (°)	94.5
Rotation step (°)	0.35
Space group	$P6_5$
Unit-cell parameters (Å)	$a = b = 158.65$, $c = 102.57$
Resolution (Å)	20–2.15
Mosaicity (°)	0.25–0.45
Total reflections	169058
Unique reflections	74806
Merging R factor (%)	7.1 (33.1)
Completeness (%)	97.4 (97.1)
Reflections with $I > 3\sigma(I)$ (%)	75.8 (56.6)
Multiplicity	2.26 (2.16)
R_{work} (R_{free})† (%)	21.4 (25.2)
No. of protein atoms	5985
No. of solvent molecules	437
No. of heteroatoms	27
R.m.s. deviations from ideal geometry	
Bonds (Å)	0.011
Angles (°)	1.6
Improper angles (°)	1.0
Dihedral angles (°)	20.3
Estimated coordinate error	
Luzzati plot (Å)	0.26
σ_A plot (Å)	0.40
Ramachandran plot‡	
Most favoured (%)	94
Allowed (%)	6
Average B factors (Å^2)	
Overall protein atoms	40.8
Main-chain protein atoms	36.6
Side-chain protein atoms	44.4
Water	43.4
PO_4^{3-}	66.2
Cl^-	49.7

(*b*) Histone-core octamer (KBr).

Crystal dimensions	2.0 × 0.2 × 0.2 mm
X-ray source	Station 9.5, SRS Daresbury, UK
Detector	MAR image plate (300 mm)
Wavelength (Å)	0.915
Temperature (K)	100
Rotation range (°)	90.0
Rotation step (°)	0.5°
Space group	$P6_5$
Unit-cell parameters (Å)	$a = b = 158.49$, $c = 102.67$
Resolution (Å)	20–2.70
Mosaicity (°)	0.40
Total reflections	12692
Unique reflections	4472
Merging R factor (%)	6.4 (25.3)
Completeness (%)	99.1 (98.2)
Reflections with $I > 3\sigma(I)$ (%)	88.9 (74.8)
Multiplicity	2.84 (2.56)

† $R = |F_{obs} - kF_{calc}|/F_{obs}|$; R_{free} corresponds to 6% of data. Structure solved by molecular replacement (Navaza, 1994) using PDB code 1hio. ‡ Geometry was analyzed with *PROCHECK* (Laskowski *et al.*, 1993).

& Read, 1996). The program computed a cross-validated σ_A estimate and the weighting scheme between the X-ray refinement target and the geometric energy function.

Corrections for a flat bulk solvent and anisotropy in the data were also applied. The σ_A-weighted maps obtained from the subsequent refined models were used for further model building. Five cycles of manual rebuilding with the program *O* (Jones *et al.*, 1991) and conventional positional refinement with NCS constraints decreased the R_{work} to 27.3% and the R_{free} to 30.6%. Different weights for symmetry restraints of NCS-related molecules were tested and those that gave the lowest R_{free} were used in further refinements. Later the two sets of histones (primed and unprimed) were refined independently and a dozen residues from the tail regions were added. The first waters were added if their electron-density peaks were greater than 2σ and if they formed at least one hydrogen bond with a protein atom or another water molecule. In the final stages, the cutoff was decreased to 1σ and molecules with a B factor above 70 Å^2 were removed. The final refined model at 2.15 Å resolution had a crystallographic R_{work} of 21.4% and an R_{free} of 25.2% and incorporated 755 amino-acid residues, 437 water molecules, five phosphate ions and 23 chloride ions. Some of the N-terminal and C-terminal residues that could not be clearly identified in the electron density were not included in the model. As evaluated by *PROCHECK* (Laskowski *et al.*, 1993), the stereochemistry yields good scores in all categories when compared with structures refined at similar resolution, with all φ/ψ values being in allowed regions of the Ramachandran plot (Ramachandran *et al.*, 1963). The solvent content of the octamers is 64.4%, corresponding to a V_M of 3.45 Å^3 Da^{-1} (Carter *et al.*, 1996). A summary of the data collection, processing and final refinement statistics for the histone octamer are given in Table 1(*a*).

2.3. Crystals in KBr

During the refinement of the structure of the histone octamers in KCl/phosphate the positions of five distinct peaks with significant electron density, corresponding to tetrahedral phosphate ions, were observed, making hydrogen-bond contacts with mainly arginine and lysine side chains, although no potassium ions could be located. Anomalously low values for the temperature factors were observed for a number of 'water' molecules bound to protein residues. They were approximately 1.5 times lower than the average B factor of C^α atoms, suggesting that these molecules could be chloride ions.

To address this issue, chloride ions were replaced by bromide ions by soaking crystals in KBr/phosphate for several weeks. Data near to the absorption edge of bromide, at a wavelength of 0.915 Å, were collected from a cryofrozen crystal on beamline 9.5 at the Daresbury Laboratory Synchrotron Radiation Source. The data were processed to a resolution of 2.7 Å using the *HKL* program suite (Otwinowski & Minor, 1997), yielding merging R values of 6.4% and approximately 25% in the 2.8–2.7 Å highest resolution shell. The data set was 99.1% complete (98.2% in the highest resolution shell), with a multiplicity of 2.84 (2.56). The percentage of reflections with $I > 3\sigma(I)$ was 88.9% (74.8%). A difference Fourier map calculated using the KCl/phosphate

data set and the KBr/phosphate data set with *FFT* (Collaborative Computational Project, Number 4, 1994), yielded 23 unique positions corresponding to bromide ion positions (unpublished program by Dr F. C. Körber). The 23 coordinates

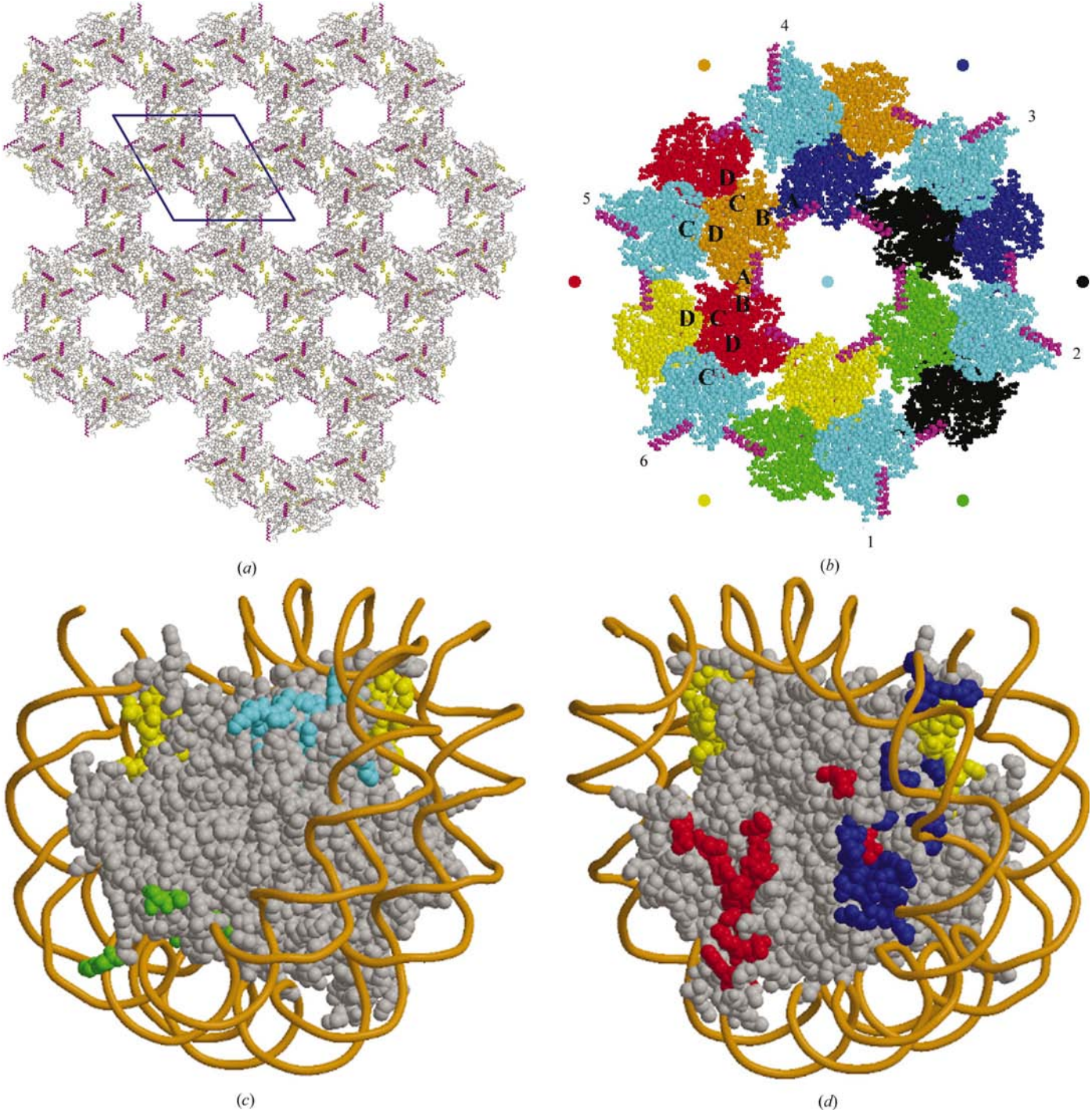

Figure 3
The packing of histone octamers in space group $P6_5$ crystals. The colour coding is common for all parts of the figures. The αC helices of the histones H2B and H2B′ are magenta and the αN helices of the histones H3 and H3′ are yellow in Figs. 3(*a*), 3(*e*) and 3(*f*). (*a*) The packing diagram viewed down *c*. The unit cell (*a*, *b*) is outlined. (*b*) The centre of the packing diagram enlarged. The octamers form left-handed helices, such as the helix shown in cyan, which interpenetrate to form the inter-octamer contacts *AB, BA, CD* and *DC* for each octamer as indicated. Each octamer is part of a helix about the centre of a solvent channel having the corresponding colour. The αC helices of histones H2B and H2B′ are shown in magenta in the figure, but only those helices for the H2Bs (as opposed to the H2B′s) are visible, facing the solvent channels. (*c*) and (*d*) DNA was positioned onto the histone octamers using the program *LSQKAB* (Kabsch, 1976) to relocate the DNA of the nucleosome-core particle accurately onto the histone octamer described herein. The figures highlight the areas of the inter-octamer contact regions, *A* (green), *B* (cyan), *C* (red) and *D* (blue) for the inter-octamer interactions. Note that whereas the *AB* interactions in the smaller contact area are exclusively between regions on the unprimed-histone face of the octamer (Fig. 3*c*), the *CD* interactions in the larger contact area are exclusively on the primed-histone face (Fig. 3*d*).

for bromide ions were compared with all the coordinates that had been assigned to the water molecules with low B values in the original KCl/phosphate coordinate file and in each case an exact correspondence was found with coordinates of a water molecule, without the need for an anomalous difference map. These positions were therefore provisionally assigned as chloride ions and a further round of refinement was carried out to determine their temperature factors. After this analysis, the provisional assignment of the 23 chloride ions was made permanent. The crystal data and refinement statistics are given in Table 1(*b*).

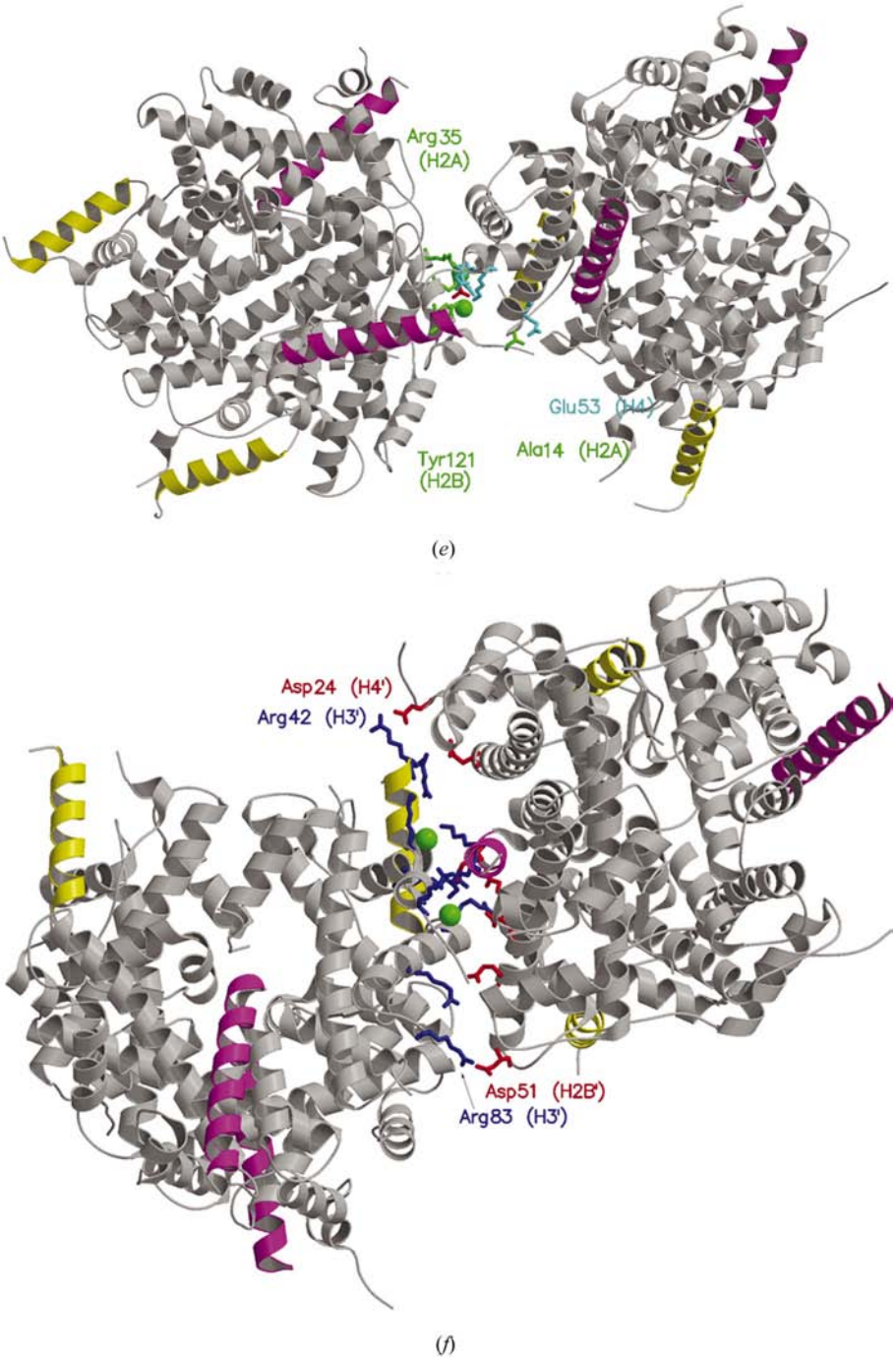

Figure 3 (continued)
The packing of histone octamers. (*e*) and (*f*). The figures show the relative orientations of the octamers in the smaller (*AB*) (Fig. 3e) and larger (*CD*) (Fig. 3*f*) interactions. The small green spheres in the interacting regions represent chloride ions and the red cross in Fig. 3(*e*) indicates the position of the phosphate. Note the red acidic region on the right-hand surface and the blue basic region on the left-hand surface of Fig. 3(*f*) (see Table 2 for details).

3. Results

3.1. Interactions between histone octamers

The chick erythrocyte histone octamer, described herein, crystallized in space group $P6_5$, with one octamer in the asymmetric unit. Fig. 3(*a*) shows a packing diagram of histone octamers, while Fig. 3(*b*) shows a detailed view of one complete helical repeat of histone octamers of pitch 102.5 Å and outer diameter 300 Å (shown in cyan) coiling about the centre of a solvent channel, indicated by the small cyan ring. The figure illustrates two pairs of interactions: a smaller area interaction (2500 Å^2) between surfaces A and B, defined in Table 2 and Fig. 3(*e*), and a larger area interaction (4000 Å^2) between surfaces C and D, defined in Table 2 and Fig. 3(*f*).

Area A involves largely basic amino-acid residues, mostly on histone H2A (Table 2), while area B involves residues from histone H4, both acidic and basic. A phosphate ion (1) and two chloride ions (d and v) are also involved. Surface C comprises the larger interaction area and involves many acidic amino-acid residues on histones H2A′, H2B′ and H4′, while area D, except for one Gly, involves basic amino-acid residues from histones H3′ and H4′. The interactions therefore are with histone octamers related by adjacent 6_5 screw axes.

The AB interaction areas are exclusively on the unprimed histones (Fig. 3*c*) whereas the CD interaction areas are on the faces of the histones formed exclusively by the primed histones (Fig. 3*d*). Table 2 shows that the AB interactions involve three hydrogen bonds plus two connections *via* chloride ions and one *via* a phosphate (Figs. 2*c* and 2*e*). The CD interactions (Table 2) involve six direct acid–base salt bridges (Figs. 2*d* and 2*f*);

Table 2
Inter-octamer distances (Å) showing the amino-acid residues involved in the smaller (*AB*) and larger (*CD*) crystal-packing surfaces (see Figs. 3*e* and 3*f*).

Table entries are grouped by type of interaction.

(*a*) Smaller-area packing interactions

A	*B*	Distance (Å)
H2A, Ala14 N	H4, Glu53 $O_{\varepsilon1}$	3.06
H2A, Arg35 NH1	H4, Gln27 O	3.12
H2B, Tyr121 OH	H4, Asp24 $O_{\delta2}$	2.56
H2A, Arg29 NH	Cl v	3.21
Cl v	H4, Lys31 N_{ζ}	3.21
H2A, Arg35 NH	Cl d	3.45
Cl d	H4, Lys31 N	3.43
H2A, Arg32 NH	PO_4, 1 O1	2.81
H2A, Lys36 N_{ζ}	PO_4, 1 O1	2.95
H2A, Arg32 NH	PO_4, 1 O2	2.76
H2A, Arg29 NH	PO_4, 1 O2	3.09
PO_4, 1 O2	H4, Lys31 N_{ζ}	2.74
H2A, Lys36 N_{ζ}	PO_4, 1 O3	3.14
H2A, Arg29 NH1	PO_4, 1 O3	2.94
H2A, Arg29 NH2	PO_4, 1 O3	3.18
PO_4, 1 O4	H4, Lys31 N_{ζ}	3.45
(PO_4, 1 O2)	(H4, Arg35 NH)	(4.64)
(PO_4, 1 O4)	(H4, Arg35 NH)	(4.68)

(*b*) Larger-area packing interactions.

C	D	Å
H2A′, Glu61 $O_{\varepsilon1}$	H3′, Arg63 N_{ε}	2.90
H2A′, Glu61 $O_{\varepsilon2}$	H3′, Arg63 NH2	2.84
H2A′, Asp90 $O_{\delta1}$	H3′, Arg63 NH2	3.03
H2A′, Asp90 $O_{\delta2}$	H3′, Arg63 NH1	3.30
H2A′, Glu91 $O_{\varepsilon1}$	H3′, Arg53 NH1	3.28
H2B′, Gln47 O	H3′, Arg72 NH1	3.20
H2B′, Val48 O	H3′, Gl*n*68 $N_{\varepsilon2}$	3.29
H2B′, Asp51 $O_{\delta2}$	H3′, Arg83 NH1	2.62
H2B′, Glu105 $O_{\varepsilon1}$	H4′, Arg36 NH2	2.92
H2B′, Glu105 $O_{\varepsilon2}$	H4′, Arg36 NH1	2.94
H4′, Glu52 $O_{\varepsilon2}$	H3′, Arg40 O	3.15
H4′, Asp24 $O_{\delta1}$	H3′, Arg42 N_{ε}	2.96
H4′, Asp24 $O_{\delta2}$	H3′, Arg42 NH2	3.37
H2B′, Lys108 N_{ζ}	Cl r	3.20
Cl r	H4′, Lys31 N	3.13
H2B′, Lys116 N_{ζ}	Cl p	2.69
Cl p	H4′, Arg23 N	3.32

two hydrogen bonds and two other connections *via* chloride ions are also involved.

The αC helix of histone H2B (Fig. 1), together with the other regions of area *A*, form prominent features on the two faces of the histone octamer. These are not involved with binding DNA in the nucleosome-core particle. Helical wheel calculations show that this α-helix has the most clearly defined hydrophilic and hydrophobic sides of all the α-helices in the histone octamer and on the unprimed face of the histone octamer it points into the solvent channel (see Figs. 3*a* and 3*b*). The residues Tyr121 and Thr122 at the end of the helix form part of area *A*. On the primed (H2A′, H2B′, H3′, H4′) face of the octamer, the αC helix of histone H2B (which is not visible in Fig. 2*b*) forms part of area C with interacting residues Glu105, Lys108 and Lys116. There are also contacts, not including hydrogen bonds, involving His109, Glu113 and Lys120 on helix αC of H2B′. Lys120 is the site of ubiquitination of histone H2B (Thorne *et al.*, 1987). The orientation of Lys120 on the primed histone-octamer face is quite different from its orientation on the unprimed histone-octamer face and other nucleosome structures. Ubiquitination of Lys120 could therefore disrupt interactions between histones such as those described above.

There is a significant distortion of the main-chain atoms in the region of the α1 helix and L1 loop of histone H3′ (Fig. 1) leading to a maximum displacement of 2 Å (main-chain oxygen of Asp77) when compared with H3. There are also some differences in the hydrogen bonding in the α1 H3′ and L1 H3′ region as a result of the extensive inter-octamer contacts in area *D*.

Fig. 3(*b*) shows that there is a minor solvent channel in the packing arrangement of the histone octamers and that the αN helix of histone H3 (Fig. 1) slopes into this channel, while the αN helix of histone H3′ is involved with the *CD* interactions.

Table 3 gives a comparison between the areas involved in crystal packing for five different histone-octamer structures: two octamers (S1 and S2) stabilized in high salt and three (S3, S4 and S5) stabilized with DNA in nucleosome core particles. There are also amino-acid residue–DNA crystal-packing interactions for the structures of Luger *et al.* (1997) and Harp *et al.* (2000). The histone octamers in ammonium sulfate (Arents *et al.*, 1991) have only half an octamer per asymmetric unit and so some of the contacts are between the H2A and H4′ docking sequences and the H2A′ and H4 docking sequences. These contacts are similar to the corresponding intra-molecular contacts for the other studies, described in §1. A detailed comparison of these five structures is made in §3.3.

Table 3 shows that the contact areas are quite different between the various studies, but a common area involves the acidic patch on the faces of the histone octamers, including the αC helices of the H2B and H2B′. In no cases are contacts between acidic and basic amino-acid residues so extensive as in our present structure (S1) (see Table 2 and Fig. 3*f*).

3.2. Phosphate ions, chloride ions and water molecules in the histone-octamer structure

3.2.1. Phosphate ions. The positions of the five phosphate ions for the histone octamer in KCl/phosphate (PO1–PO5 in PDB file 1hq3) and the amino-acid residues interacting with them are shown in Fig. 1. Residues in the amino-acid sequence that interact with DNA in the nucleosome-core particle model of Harp *et al.* (2000), from chick erythrocyte cell nuclei, are shown in red in line 2 of Fig. 1. It is clear that the phosphate ions, shown in red in line 1 in Fig. 1, interact largely with lysine and arginine residues at five different sites that, in the nucleosome-core particle, interact with DNA. The same conclusion follows from comparing our histone octamer structure with the structure of Luger *et al.* (1997).

Phosphate ions 1 and 3 are in very similar positions on either side of the octamer and the same is true of phosphate ions 2 and 4. Phosphate ion 5 interacts with Arg36 of histone H4 and does not have an equivalent on the pseudo-symme-

Table 3
Histone regions with inter-histone-octamer interactions for five crystal structures.

S1, the octamer KCl/phosphate crystals (described herein; PDB code 1hq3); S2, the octamer ammonium sulfate crystals (Arents *et al.*, 1991; PDB code 2hoi); S3, nucleosome-core particle crystals (Luger *et al.*, 1997; PDB code 1aoi); S4, nucleosome-core particle crystals (Harp *et al.*, 2000; PDB code 1eqz); S5, nucleosome-core particle crystals (White *et al.*, 2001; PDB code 1id3). Although each of the elements of structure of the histone octamers (see Fig. 1) contain different numbers of amino-acid residues, the residues involved in packing interactions have been grouped into three equal parts for a given element of structure: beginning, b; middle, m; end, e. This helps to define an approximate distribution of residues that take part in intermolecular crystal-packing interactions for overall comparison between the different crystal structures. (Note that structures S1, S3, S4 and S5 all have one octamer per asymmetric unit: each octamer has pseudo-twofold symmetry and asymmetric packing interactions. In S2 there is half an octamer per asymmetric unit and so there is equivalence between the primed and unprimed histones in any chosen octamer. The docking interactions for S1, S3, S4 and S5 become part of the inter-octamer interactions in S2 and these interactions are shown in italics in S2.)

		S1	S2	S3	S4	S5			S1	S2	S3	S4	S5
H2A	N-terminal tail	e			bme		H2A′	N-terminal tail				bm	
H2A	αT Helix	b					H2A′	αT Helix					
H2A	L_N						H2A′	L_N					
H2A	α1 Helix	me	e				H2A′	α1 Helix		e			
H2A	L1	e					H2A′	L1					
H2A	α2 Helix			me	me	m	H2A′	α2 Helix	me				e
H2A	L2		b				H2A′	L2		b			b
H2A	α3 Helix		b				H2A′	α3 Helix	e	b			
H2A	*α3a* Helix			b	b		H2A′	*α3a* Helix	b				
H2A	Docking sequence		*bme*				H2A′	Docking sequence		*bme*			
H2A	C-terminal tail						H2A′	C-terminal tail			b	bme	
H2B	N-terminal tail						H2B′	N-terminal tail				m	
H2B	α1 Helix			m	e		H2B′	α1 Helix	e				
H2B	L1						H2B′	L1	b			b	bm
H2B	α2 Helix		*m*e				H2B′	α2 Helix		*m*e			
H2B	L2						H2B′	L2					
H2B	α3 Helix						H2B′	α3 Helix			b		
H2B	α_C Helix	e	bme	bm	b e	bme	H2B′	α_C Helix	bme	bme		me	me
H3	N-terminal tail				e		H3′	N-terminal tail	e		me	me	
H3	αN Helix		m*e*				H3′	αN Helix	b e	m*e*			
H3	L_N		b				H3′	L_N		b			
H3	α1 Helix	bm		m	e		H3′	α1 Helix	bm		e	e	
H3	L1			m	m		H3′	L1	m				
H3	α2 Helix		*b* e	m			H3′	α2 Helix	b	*b* e			
H3	L2						H3′	L2					
H3	α3 Helix		b			b	H3′	α3 Helix		b			
H4	N-terminal tail	e			e		H4′	N-terminal tail	e		me	e	
H4	αT Helix	b m					H4′	αT Helix	bme			b	
H4	α1 Helix	b	m				H4′	α1 Helix	m	m			
H4	L1						H4′	L1					
H4	α2 Helix	b				m	H4′	α2 Helix	b				
H4	L2						H4′	L2					
H4	α3 Helix						H4′	α3 Helix					
H4	Docking sequence		*bme*				H4′	Docking sequence		*bme*			

trical part of the octamer, because Arg36 of H4′ is part of the *CD* inter-octamer packing region (see Table 2).

Figs. 4(*a*) and 4(*b*) illustrate the interactions involved with phosphate ions 1 and 3, respectively, showing how the phosphate ions can bind several basic amino-acid residues, thus performing, in the absence of DNA, a similar role to DNA phosphates. However, the side chains of the interacting amino-acid residues are structured quite differently from those interacting with DNA. The details of the interaction of these residues with nucleosome-core particle DNA have been discussed by Luger & Richmond (1998) and Harp *et al.* (2000). In Fig. 4(*a*), Lys31 of histone H4 is from an adjacent histone octamer. Potassium ions were not observed in the electron-density map.

3.2.2. Chloride ions. 23 chloride ions were located as described in §2 by comparing results from crystals in KCl/phosphate and KBr/phosphate. Four of the chloride ions: d, v, p and r (Fig. 1) are involved in the inter-octamer packing interactions described in §3.1 and Table 2. The chloride ions are coded in green in Fig. 1 (line 1) above their interacting amino-acid residues. Chloride ions d and v also interact with arginines that, in the nucleosome, would be in DNA-binding regions, while p and r interact with lysines.

Six further chloride ions (see Fig. 1), c, i, j, k, l and o, bind to regions that in the nucleosome would be DNA-binding regions. Chloride ions c, k and l interact directly with arginines, while the other three interact with amino-acid residues next to arginines. The chloride ions i and o engage in similar interactions on either side of the octamer and the same is true of chloride ions c and j. Fig. 5(*a*) shows how chloride ion k interacts with two arginines and a glutamine.

Four chloride ions, b, f, g and h (Fig. 1, line 1), are in exactly the same positions as those detected in the nucleosome-core particle structures, two by Harp *et al.* (2000) and four by Davey *et al.* (2002), and may therefore be part of the fundamental structure of the nucleosome. However, estimates of typical chloride-ion concentrations in cell nuclei are likely to be much less than 100 m*M* (Dick, 1978), whereas the chloride-

ion concentration in the nucleosome-core particle crystals is 114 m*M* (Luger *et al.*, 1997), with a much higher level of 2 *M* in our octamer crystals. Chloride ions b and f are in similar positions in the octamer, interacting with Gly46 of the H2As and Ser91 of H2Bs, close to the L1–L2 DNA-interacting sites of the nucleosome-core-particle studies. Chloride ions g and h are also in symmetrical positions, binding to Lys122 on the H3 histones.

There are four chloride ions in the octamer in KCl/phosphate that are in two symmetrical pairs but are not reported in the analysis of nucleosome-core particle crystals: chloride ion e is symmetrical with q and chloride ion w is symmetrical with n (Fig. 1). Fig. 5(*b*) shows the interactions involving chloride ion q, which increases the interactions between the H2A docking sequence at Thr101 and the H4′ docking sequence at Arg95. The side-chain orientations of these two residues in the nucleosome-core particle structure of Luger *et al.* (1997) are different from those in the KCl/phosphate octamer, but this is not true in comparison with the structure of Harp *et al.* (2000). There is a minor difference in sequence near to this region of the octamer, where Lys99 of each histone H2A is replaced by an Arg99 in the Luger *et al.* (1997) *Xenopus laevis* histone sequence.

Fig. 5(*c*) illustrates the docking region involving the chloride ions q and w. There are two short parallel β-sheets shown in the figure: the one on the right of the figure is in the L1–L2 (H2B′–H2A′) DNA-binding site (similar β-sheets occur in all eight of these positions in the octamer in KCl/phosphate; see Fig. 1) and the second is the β-sheet of the interaction between the H4–H2A′ docking sequences described in §1. The figure shows water molecules and chloride ion w which interacts between H4 Gly101 and H2B′ Ser64. This interaction plus several other interactions with water molecules couples the last few residues of the H4 docking sequence to the α2 helix of the histone H2A′. The structure of the octamer in ammonium sulfate of Arents *et al.* (1991) and of the octamer in the two nucleosome-core particle studies of Luger *et al.* (1997) and Harp *et al.* (2000) differ from that of the octamer in KCl/phosphate in these last three or four residues of histones H4 (Fig. 6). However, the interactions in the latter case are consistent, as they are in symmetrical positions.

Thus far, 18 of the 23 chloride ions have been accounted for. The remaining five chloride ions: a, m, s, t and u, do not have symmetrical equivalents in the histone octamer (Fig. 1, line 1). However, chloride ion s interacts directly with an arginine, while chloride ions m and u interact with residues next to arginines. The total number of basic amino-acid residues found to be interacting with the chloride and phosphate anions is 21 (Fig. 1).

3.2.3. Water molecules. Figs. 2(*c*) and 5(*c*) show the water molecules associated with the H4 (H4′) and H2A′ (H2A) docking sequences. Many of the amino-acid residues of the Harp *et al.* (2000) structure contain water molecules in common with the present study and the cross-linking properties of water molecules reported in the paper of Davey *et al.* (2002) are evident, particularly in the docking interactions of the molecular cluster of Fig. 2(*c*) and the docking interactions of Fig. 5(*c*). Of the 437 water molecules located in our present structure, 322 form hydrogen bonds to protein, while the remaining 115 interact with other water molecules to form solvent clusters. In total there are 585 water contacts. This includes contacts between adjacent water molecules.

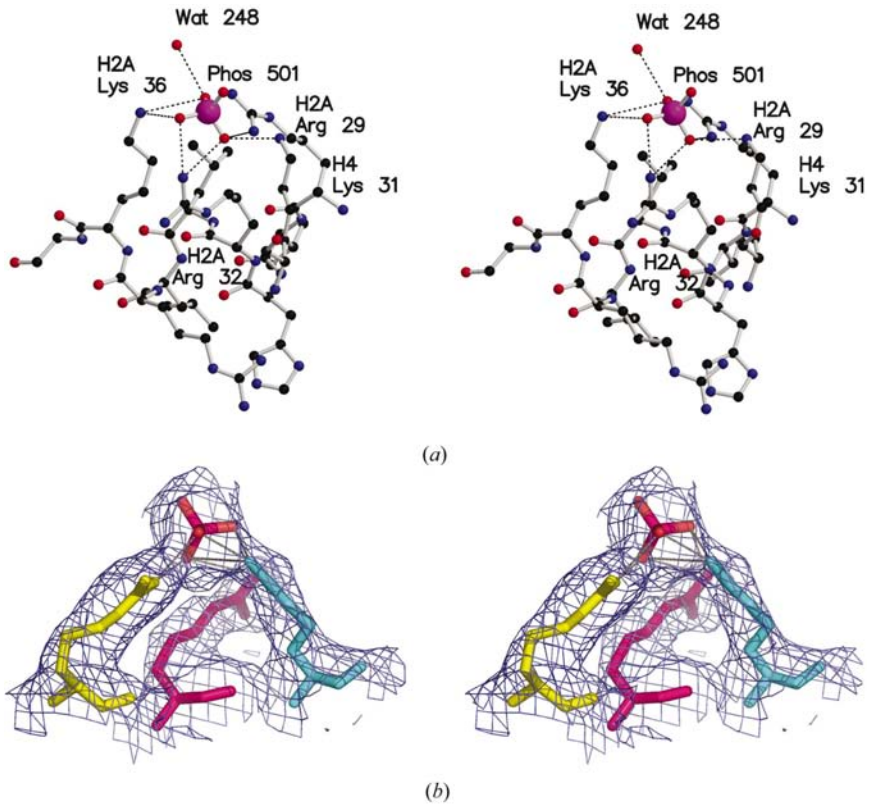

Figure 4
Stereo figures of amino-acid residues interacting with phosphates 1 and 3. (*a*) Interactions between amino-acid residues and phosphate 1 (see Fig. 1). Some interactions occur between octamers, so that H4 Lys31 is from a neighbouring molecule. See also Table 3. (*b*) Amino-acid residues binding to phosphate 3 (see Fig. 1). The tetrahedral phosphate group is shown in red and the amino-acid residues are histone H2A′ Arg32, magenta; Arg29, yellow; Lys36, cyan. Interaction distances between the amino-acid residues and phosphate 3 are as follows: H2A′ Arg29 (α1) NH1 with phosphate O4, 2.58 Å; H2A′ Arg29 (α1) NH1 with phosphate O3, 2.89 Å; H2A′ Lys36 (α1) N^{ζ} with phosphate O4, 3.58 Å; H2A′ Lys36 (α1) N^{ζ} with phosphate O2, 2.70 Å; H2A′ Lys 36 (α1) N^{ζ} with phosphate O3, 2.56 Å; H2A′ Arg32 (α1) NH2 with phosphate O2, 3.03 Å; H2A′ Arg32 (α1) NH2 with phosphate O4, 3.55 Å.

3.3. Structure comparisons

The program *LSQKAB* (Kabsch, 1976) was used to reorient compatible regions within the different molecules to a common origin and orientation and also to calculate the r.m.s. positional difference between

corresponding atoms. Differences in the octamer in KCl/phosphate, in ammonium sulfate (Arents *et al.*, 1991) and in the nucleosome-core particle (Luger *et al.*, 1997; Harp *et al.*, 2000) have already been described in the context of the packing of the octamers and nucleosome-core particles and the effect of ions on the structures. Clearly there are many differences in side-chain orientations between the structures as a result of these differences in packing and ion binding. The only differences in main-chain structures, when comparing the higher resolution nucleosome-core particle studies of Luger *et al.* (1997) and Harp *et al.* (2000) and the present work, are in the last few residues of histone H4 and the distortion in structure arising from the molecular packing described in §3.1.

The docking of the histones (H2A–H2B) (and H2A′–H2B′) against the histones (H3′–H4′) (and H3–H4) is highly consistent between the different structures, both in the main-chain and the side-chain positions. This is shown clearly in Fig. 6, where four structures [nucleosome-core particles (Luger *et al.*, 1997, Harp *et al.*, 2000) and histone octamers (Arents *et al.*, 1991 and the present study)] have been overlaid, so that the docking sequences of histones H4 and H2A′ can be compared. All the structures are virtually the same including side chains except in the region of the differences in H4 structure discussed earlier.

The histone octamer is designed to position the histone-tail end amino-acid residues correctly as well as the C-terminal tails of the histones H2A. This is achieved by the locking of α-helices as described in §1. If we compare the main-chain and side-chain structures of these helices together using the program *LSQKAB* (Kabsch, 1976) there is good agreement between the structures. In comparing main-chain structures, excluding the last five residues of the H4s and the region of distortion owing to the packing of octamers described in §3.1, the program gives an r.m.s. deviation of only 0.57 Å when comparing the structure of Luger *et al.* (1997) with the structured region of the octamer in KCl/phosphate. The structured region is defined by the following residues: for H2As, 17–115; for H2Bs, 38–123; for H3s, 43–131; for H4s, 25–92. Together, these residues define the octamer without tails. The buried hydrogen-bond cross-tie distances in the H3–H3′, H2B–H4 and H4′–H2B′ four-helix bundles for the octamer in KCl/phosphate and the distance between the two cysteine S atoms (6.1 Å) are in good agreement with the structure of Luger *et al.* (1997).

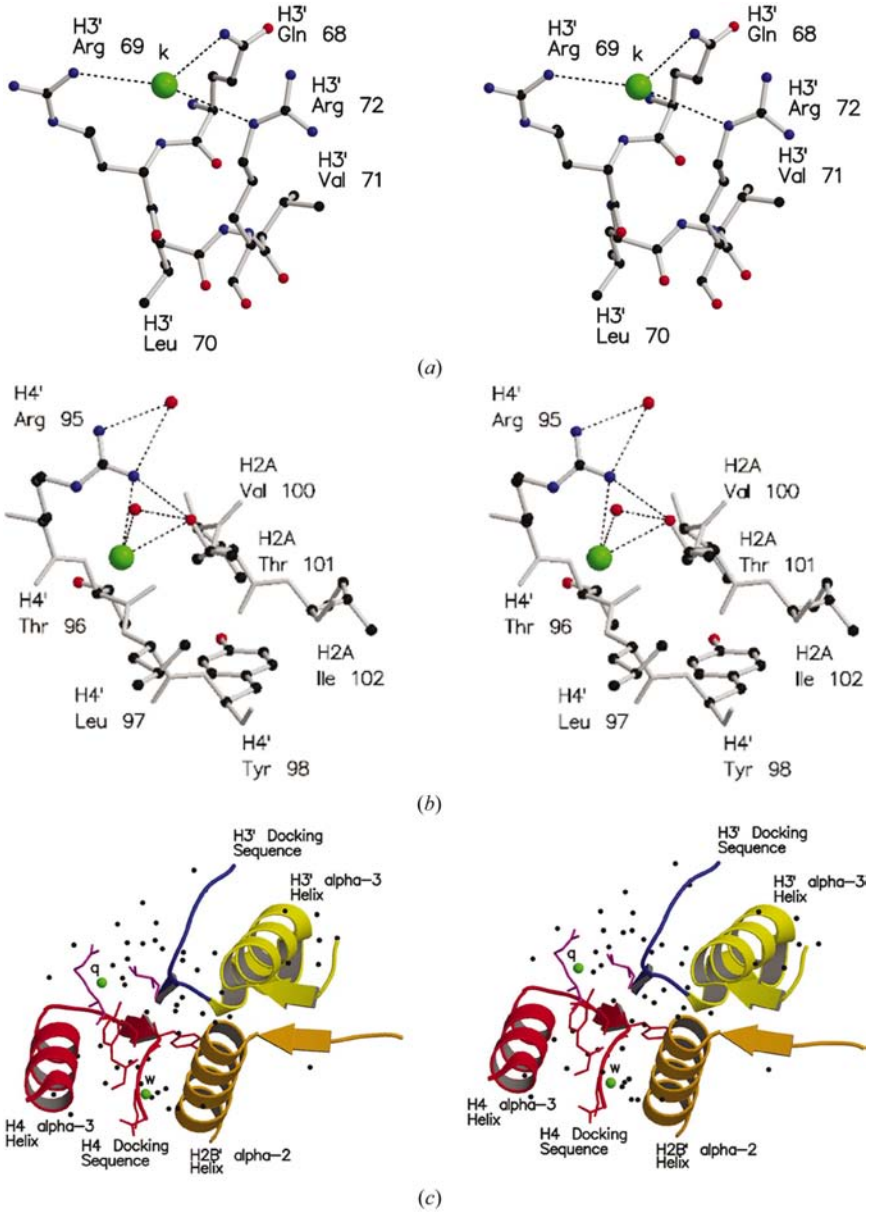

Figure 5
Stereo figures of amino-acid residues interacting with chlorides a. Interactions of chloride k with Arg69, Arg72 and Gln68 in histone H3′ (see also Fig. 1). (*b*) The extra interaction between the docking sequence of histone H4′ at Arg95 and the docking sequence of histone H2A at Thr101, involving chloride q (green) and water molecules (black). Note the short parallel-β structure coupling residues Val100, Thr101 and Ile102 of histone H2A to residues Thr96, Leu97 and Tyr98 of histone H4′. (*c*) Chloride q provides the extra inter-docking sequence interaction of Fig. 4(*b*) and chloride w and water molecules provide the coupling between the H4 docking sequence and the α2 helix of histone H2B′. Note the two parallel β-sheet regions. Chloride ions are shown in green and water molecules in black.

4. Discussion

There are many processes involving nucleosomes, structural proteins and enzyme complexes that regulate chromatin function in eukaryotic cells throughout their cell cycles (Wu & Grunstein, 2000). Although there is still much work to be performed in order to fully understand the mechanisms occurring in these processes, some of them will involve interactions

between histone octamers which may act in undermining DNA contacts during the process of spooling. Nucleosome remodelling for transcription, for example, can lead to the formation of di-nucleosomes where DNA has been partially unwound (Lorch *et al.*, 2001). Further, the capture of a histone octamer by an octamer on the other side of RNA polymerase during transcription could involve octamer–octamer interactions, since transfer of histone octamers around the polymerase has been reported (Studitsky *et al.*, 1994; Bednar *et al.*, 1999). As discussed in §3.2.2, caution must be exercised when comparing physiological chloride ion concentrations with the high salt levels required for stabilization of octamers *in vitro*. Consequently, this means the inter-octamer crystal-packing interactions cannot be assumed to be relevant *in vivo*. However, the large-area interaction (*C* to *D* in Table 2) does involve many salt bridges and, as discussed by others (Luger *et al.*, 1997; White *et al.*, 2001), the acidic patch on the H2A′, H2B′, H4′ face of the octamer is likely to be involved in interactions of functional importance. Although this patch is not involved with DNA binding, its functional importance is indicated by a highly conserved sequence in this region.

Four symmetry-related chloride ions of the histone-octamer structure in KCl/phosphate are also present in the nucleosome-core particles and it is possible that they form an important part of the structure *in vivo* (see §3.2.2). However, even in the case of the nucleosome-core particle crystals, the chloride ion concentration is significantly above physiological levels, as discussed above. There are a further four pairs of symmetrically placed chloride ions in the octamer, two pairs of which do not bind to regions of the octamer; however, in the nucleosome they would bind to DNA. The extra interaction between the docking sequences mediated by a chloride ion in each case (Figs. 5*b* and 5*c*) is absent in nucleosome-core particle crystals. These chloride ions may well be instrumental in stabilizing the interactions between the (H2A–H2B) dimers and the $(H3–H4)_2$ tetramers in the high-salt octamer in the absence of DNA. The pair of chloride ions locking the end amino-acid residues of H4 (H4′) to the α2 helix of H2B′ (H2B) may also be imposed by the high chloride content of our crystals.

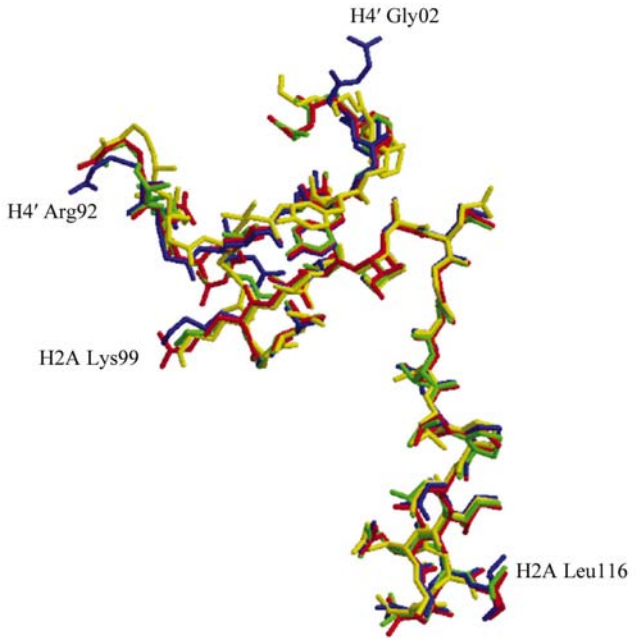

Figure 6
Superposition of the H2A (residues 97–116) and H4′ (residues 92–102) docking sequences for the following octamer structures: S1, the octamer in KCl/phosphate (blue); S2, the octamer in ammonium sulfate of Arents *et al.* (1991) (yellow); S3, the octamer in the nucleosome core particle of Luger *et al.* (1997) (red); S4, the octamer in the nucleosome core particle of Harp *et al.* (2000) (green). Notice the similarity between the structures as well as some differences, particularly for histone H4′.

The octamer is stable in high salt, but dissociates into two (H2A–H2B) dimers and an $(H3–H4)_2$ tetramer (not two dimers) at low ionic strength in the absence of DNA (Eickbush & Moudrianakis, 1978). At high ionic strength, ions such as the chlorides and phosphates described herein bind to charged lysines and arginines in a manner that could mimic the much more specific binding of the DNA in the nucleosome. These interactions could be stabilizing the octamers in our crystal structure.

The structure of the histone octamer is such that there are no contacts between the (H3–H4) and (H3′–H4′) components of the histone tetramer except in the neighbourhood of the H3–H3′ four-helix bundle and there are no contacts between the histone dimer (H2A–H2B) and the (H3–H4) part of the histone tetramer except in the neighbourhood of the H2B–H4 four-helix bundle. Moreover, there is only one contact between the (H2A–H2B) and (H2A′–H2B′) dimers at the L1 loops of the H2As (see Fig. 2*b*) and the (H2A–H2B) dimers do not make contact with the (H2A′–H4′) part of the histone tetramer except *via* the H2A and H4′ docking sequences. Therefore, the connections between the histone (H2A–H2B) dimers and the (H3–H4) tetramers are essentially only *via* the H2B–H4 four-helix bundles and the docking sequences. The dissociation of the histone octamer at low ionic strength only involves these two groups of interactions. The H2A docking sequence (Fig. 1) contains one lysine, four polar amino-acid residues and 14 apolar residues. Similarly, the H4 docking sequence contains one arginine, two polar amino-acid residues and six apolar residues. In our view, it is the apolar nature of these docking sequences and the characteristics of the H2B–H4 four-helix bundles that account for the histone-octamer dissociation at low ionic strength. High salt concentrations strengthen the interactions between hydrophobic surfaces; therefore, one would expect destabilization of hydrophobic interactions at lower salt. Indeed, this is the principle of hydrophobic interaction chromatography. Histone-fold pairing is *via* hydrophobic interactions, as is the binding of the αC helices to the rest of the (H2A–H2B) dimers; however, clearly the pairing persists at lower ionic strengths than those where the histone octamers dissociate. The histone-sequence variant H2A.Z has been correlated with actively transcribed chromatin and Suto *et al.* (2000) have studied nucleosome-core particle crystals containing this variant. The key role of the H2A docking sequence discussed above is demonstrated in this work and distinct localized changes result in subtle

destabilization of the interaction between the (H2A.Z–H2B) dimer and the $(H3–H4)_2$ tetramer.

We are grateful to Dr Fritjof Körber, Dr Pierre Rizkallah, Dr Steven Prince, Dr Dean Myles, Dr Miroslav Papiz and Dr Katherine McAuley for many helpful discussions, support with X-ray facilities at Daresbury Laboratory, comments on the manuscript and support with molecular graphics. We acknowledge support from John Moores University and the work forms part of the Daresbury Laboratory Collaborative Research Program. The EPSRC of the UK gave support with a collaborative research grant. Figures were produced using *RASMOL* (Sayle & Millnerwhite, 1995), *MOLSCRIPT* 2.0 (Kraulis, 1991), *Raster3D* (Merritt & Bacon, 1997) and *PYMOL* (DeLano Scientific). We thank the referees for their many helpful comments. Harrisons Poultry, Antrobus, Cheshire kindly provided chicken blood.

References

Akey, C. W. & Luger, K. (2003). *Curr. Opin. Struct. Biol.* **13**, 6–14.
Arents, G., Burlingame, R. W., Wang, B. C., Love, W. E. & Moudrianakis, E. N. (1991). *Proc. Natl Acad. Sci. USA*, **88**, 10148–10152.
Bednar, J., Studitsky, V. M., Gregoryev, S. A., Felsenfeld, G. & Woodcock, C. L. (1999). *Mol. Cell*, **4**, 377–386.
Brünger, A. T., Adams, P. D., Clore, G. M., DeLano, W. L., Gros, P., Grosse-Kunstleve, R. W., Jiang, J. S., Kuszewski, J., Nilges, M., Pannu, N. S., Read, R. J., Rice, L. M., Simonson, T. & Warren, G. L. (1998). *Acta Cryst.* D**54**, 905–921.
Carter, R. J., Lambert, S. J., Chantalat, L., Körber, F. C. F., Nicholson, J. M. & Baldwin, J. P. (1996). *Acta Cryst.* D**52**, 569–570.
Collaborative Computational Project, Number 4 (1994). *Acta Cryst.* D**50**, 760–763.
Davey, C. A., Sargent, D. F., Luger, K., Maeder, A. W. & Richmond, T. J. (2002). *J. Mol. Biol.* **319**, 1097–1113.
Dick, D. A. (1978). *J. Physiol.* **284**, 37–53.
Eickbush, T. H. & Moudrianakis, E. N. (1978). *Biochemistry*, **17**, 4955–4964.
Finch, J. T & Klug, A. (1976). *Proc. Natl. Acad. Sci. USA*, **73**, 1897–1901.
Harp, J. M., Hanson, B. L., Timm, D. E. & Bunick, G. J. (2000). *Acta Cryst.* D**56**, 1513–1534.
Jones, T. A., Zou, J-.Y., Cowan, S. W. & Kjeldgaard, M. (1991). *Acta Cryst.* A**47**, 110–119.
Kabsch, W. (1976). *Acta Cryst.* A**32**, 922–923.
Kraulis, P. J. (1991). *J. Appl. Cryst.* **24**, 946–950.
Lambert, S. J., Nicholson, J. M., Chantalat, L., Reid, A. J., Donovan, M. J. & Baldwin, J. P. (1999). *Acta Cryst.* D**55**, 1048–1051.
Laskowski, R. A., MacArthur, M. W., Moss, D. S. & Thornton, J. M. (1993). *J. Appl. Cryst.* **26**, 283–291.
Lorch, Y., Zhang, M. & Kornberg, R. D. (2001). *Mol. Cell*, **7**, 89–95.
Luger, K., Maeder, A. W., Richmond, R. K., Sargent, D. F. & Richmond, T. J. (1997). *Nature (London)*, **389**, 251–260.
Luger, K. & Richmond, T. J. (1998). *Curr. Opin. Struct. Biol.* **8**, 33–40.
Merritt, E. A. & Bacon, D. J. (1997). *Methods Enzymol.* **277**, 505–524.
Moehs, C. P., Baxevanis, A. D., Moudrianakis, E. N. & Spiker, S. (1992). *Biochemistry*, **31**, 10844–10851.
Navaza, J. (1994). *Acta Cryst.* A**50**, 157–166.
Otwinowski, Z. & Minor, W. (1997). *Methods Enzymol.* **276**, 307–326.
Pannu, N. S. & Read, R. J. (1996). *Acta Cryst.* A**52**, 659–668.
Ramachandran, G. N., Ramakrishnan, G. & Sasisekharan, V. (1963). *J. Mol. Biol.* **7**, 95–99.
Rice, J. C. & Allis, C. D. (2001). *Curr. Opin. Cell Biol.* **13**, 263–273.
Richmond, T. J., Finch, J. T., Rushton, B., Rhodes, D. & Klug, A. (1984). *Nature (London)*, **311**, 532–537.
Sayle, R. A. & Milnerwhite, E. J. (1995). *Trends Biochem. Sci.* **20**, 374–376.
Studitsky, V. M., Clark, D. J. & Felsenfeld, G. (1994). *Cell*, **76**, 371–382.
Suto, R. K., Clarkson, M. J., Tremethick, D. J. & Luger, K. (2000). *Nature Struct. Biol.* **7**, 1121–1124.
Thoma, F., Koller, T. & Klug, A. (1979). *J. Cell Biol.* **83**, 403–427.
Thorne, A. W., Sautiere, P., Briand, G. & Crane-Robinson, C. (1987). *EMBO J.* **6**, 1005–1010.
Wang, B., Rose, J., Arents, G. & Moudrianakis, E. N. (1994). *J. Mol. Biol.* **236**, 179–188.
White, C. L., Suto, R. K. & Luger, K. (2001). *EMBO J.* **20**, 5207–5218.
Wolffe, A. P. (1999). *Chromatin Structure.* New York: Academic Press.
Woodcock, C. L. & Dimitrov, S. (2001). *Curr. Opin. Genet. Dev.* **11**, 130–135.
Wu, J. & Grunstein, M. (2000). *Trends Biochem. Sci.* **25**, 619–623.